NANO LETTERS

Letter

pubs.acs.org/NanoLett

Dynamic Control of Plasmon Generation by an Individual Quantum System

Christoph Große,*[,†] Alexander Kabakchiev,[†] Theresa Lutz,[†] Romain Froidevaux,[†,∥] Frank Schramm,[‡] Mario Ruben,[‡,§] Markus Etzkorn,[†] Uta Schlickum,[†] Klaus Kuhnke,[†] and Klaus Kern[†,∥]

[†]Max-Planck-Institut für Festkörperforschung, Heisenbergstraße 1, 70569 Stuttgart, Germany

[‡]Karlsruher Institut für Technologie (KIT), Institut für Nanotechnologie, 76344 Eggenstein-Leopoldshafen, Germany

[§]IPCMS-CNRS, Université de Strasbourg, 67034 Strasbourg, France

[∥]Ecole Polytechnique Fédérale de Lausanne, 1015 Lausanne, Switzerland

Supporting Information

ABSTRACT: Controlling light on the nanoscale in a similar way as electric currents has the potential to revolutionize the exchange and processing of information. Although light can be guided on this scale by coupling it to plasmons, that is, collective electron oscillations in metals, their local electronic control remains a challenge. Here, we demonstrate that an individual quantum system is able to dynamically gate the electrical plasmon generation. Using a single molecule in a double tunnel barrier between two electrodes we show that this gating can be exploited to monitor fast changes of the quantum system itself and to realize a single-molecule plasmon-generating field-effect transistor operable in the gigahertz range. This opens new avenues toward atomic scale quantum interfaces bridging nanoelectronics and nanophotonics.

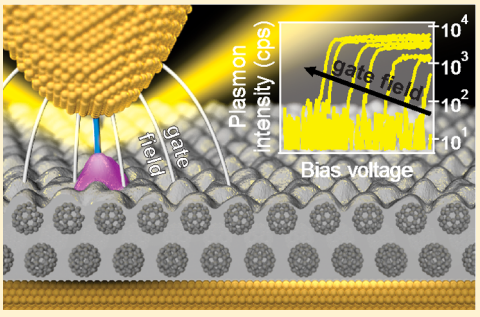

KEYWORDS: *Plasmonics, STM-induced luminescence, time-dependent STM, Ir(ppy)$_3$, plasmon gating*

Plasmons, collective density oscillations of the conduction electrons of metals, are the key to guide and manipulate light on the nanoscale.[1] The electromagnetic waves arising at the metal surface, known as surface plasmon polariton (SPP) modes, allow a confinement to structures far below the diffraction limit of light.[2] This can be used, for example, for extreme light concentration,[3] optically operating computer chips with unprecedented processing speeds[4,5] or highly sensitive sensors.[6] Beyond that, there is a growing interest in studying and exploiting the quantum nature of plasmons,[7,8] for instance, as information carriers in quantum communication and quantum computing.[9−11]

Typically, SPPs are excited by coupling incident light via prisms, gratings, or optical antennas to the plasmons of a metal surface. While this allows the generation of individual SPP quanta,[8] the diffraction limit of the exciting photons remains; hence, two independently driven plasmon sources require a distance of several hundred nanometers. This can be circumvented by bringing the plasmonic structure in close proximity to a localized light source and exploiting its near-field.[12] However, such plasmon-emitting diodes[13−16] and transistors[17] contain a multitude of emitting centers and have not been realized in the single quantum regime yet. An alternative is the excitation of plasmons by inelastically tunneling electrons in tunnel junctions.[18] Various scanning tunneling microscopy (STM) studies have shown that such junctions can be scaled down to the atomic level[19,20] and enable launching of propagating SPPs on metal surfaces,[21] metallic nanowires,[22] and graphene.[23]

Here, we demonstrate that an individual quantum system, consisting of a single *fac*-tris(2-phenylpyridine)iridium(III), Ir(ppy)$_3$, molecule in a double tunnel barrier between two gold electrodes (Figure 1), is able to dynamically gate the electrical plasmon generation in the junction. Depending on the energy alignment of its electronic levels, the quantum system either blocks or permits the current through and the plasmon excitation in the junction.[24] Thus, subtle changes of the quantum system can result in strong variations in the plasmon intensity. We demonstrate that this highly sensitive gating works in two ways: On the one hand, it enables following fast dynamic changes of the quantum system itself by detecting the excited plasmons. On the other hand, weak external manipulations of the quantum system allow a dynamic control of the plasmon generation at its quantum limit.

Specifically, we use the energy shift of a molecular state induced by an electric field.[25] By this means, we realize a single-molecule plasmon-generating field-effect transistor: As soon as the electric field at the molecule surpasses a specific threshold, the transistor turns on and the tunnel current between the source and drain electrode (I_{SD}) as well as the intensity of plasmons (P) generated in the junction rise by several orders of

Received: June 27, 2014
Revised: August 22, 2014
Published: September 2, 2014

   dx.doi.org/10.1021/nl502413k | *Nano Lett.* 2014, 14, 5693−5697

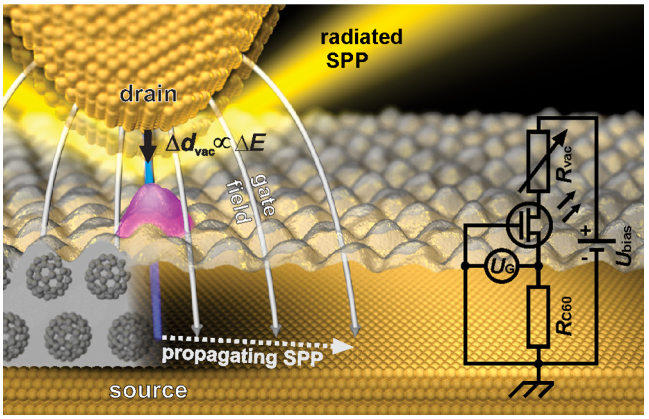

Figure 1. Gating of the electrical plasmon generation by an individual molecule. The gating is achieved by a single $Ir(ppy)_3$ molecule (magenta) in a vacuum/C_{60} bilayer double tunnel barrier. The molecule is contacted via the gold substrate beneath (source) and a gold STM tip (drain). Above a specific electric field and thus gate voltage (U_G), surface plasmon polariton (SPP) modes are excited by electrons (blue) tunneling through the junction. These SPPs either propagate along the surfaces of the electrodes or radiate as light (yellow beam). The electric field and thus the gate voltage are controlled via the spacing d_{vac} between the molecule and the drain contact. An equivalent circuit diagram is shown on the right-hand side.

magnitude. The electric field is regulated by varying the thickness of the vacuum barrier (d_{vac}), that is, the molecule–drain distance at a constant bias voltage (see Figure 1). Hence, it is possible to adjust the electric field in the junction and the tunnel voltage independently from each other. In order to precisely control d_{vac} and measure I_{SD}, we employ a scanning tunneling microscope working at a temperature of 4 K. Concurrently, we profit from the fact that the STM tip acts as an antenna, which converts plasmons excited in the nanoscopic tunnel junction to photons emitted and detected in the far-field (see Supporting Information, Figure S1).

Figure 2a,b present the measured plasmonic light intensity, P, and the source–drain current, I_{SD}, respectively, as a function of the applied voltage, U_{bias} and the molecule–drain distance, d_{vac}. In contrast to the convention common in STM studies, the bias voltage, U_{bias}, denotes the drain (tip) potential with respect to the grounded source (substrate). Both data sets in Figure 2a,b are measured simultaneously by sweeping U_{bias} at different d_{vac}, with the STM tip positioned above a single $Ir(ppy)_3$ molecule (Supporting Information, Figure S2). The absolute distance d_{vac} is determined by the procedure described in Figure S3. As an example, Figure 2c,d shows a section of P and I_{SD} as a function of U_{bias}, and the electric field strength (E) in the junction (for details see Supporting Information). At a bias voltage of ~3 V, P and I_{SD} abruptly rise by several orders of magnitude.

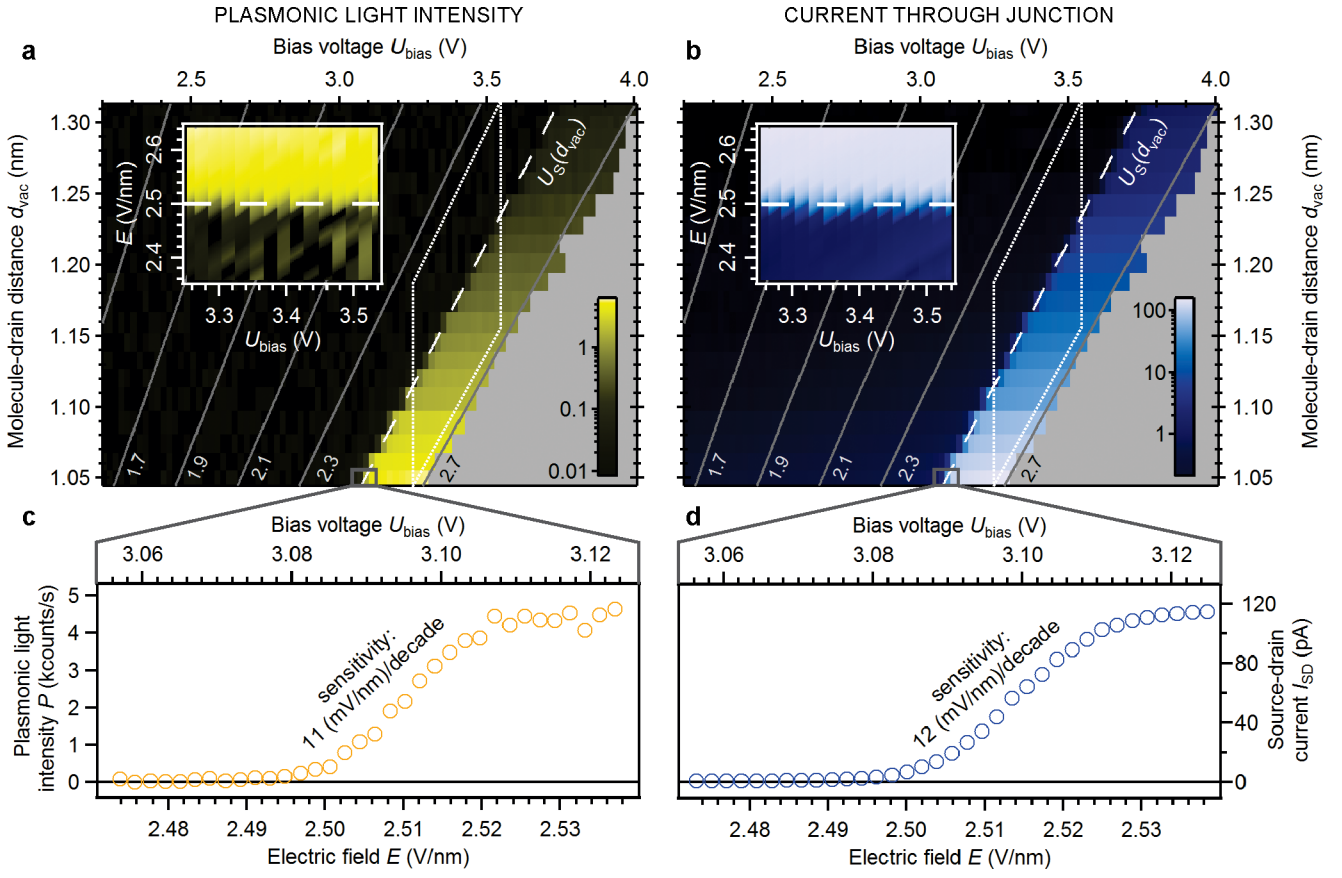

Figure 2. Field dependence of the plasmonic light intensity and the tunnel current through the junction. (a) Color-coded logarithmic plot of the measured plasmonic light intensity (in kcounts/s) and (b) the source–drain current (in pA) as a function of the applied bias voltage and the molecule–drain distance. The diagonal lines represent lines of constant electric field strength in the vacuum barrier (in V/nm). The insets show the data within the white dotted rhomboid plotted as a function of U_{bias} and E and divided by the current at the corresponding switching voltage, $U_s(d_{vac})$ (in arbitrary units). The small gray rectangles at the bottom mark the section of the plasmonic light intensity displayed in (c) and the source–drain current in (d) at the minimum d_{vac}, respectively. In (a,b) data are binned over 10 points along U_{bias}.

dx.doi.org/10.1021/nl502413k | *Nano Lett.* 2014, 14, 5693–5697

In the following, we demonstrate that the crucial parameter determining this rise is not the applied voltage but the electric field in the junction. As visible by the white dashed line in Figure 2a,b, the switching voltage $U_s(d_{vac})$, assigned to the steepest rise in I_{SD}, shifts linearly with the molecule−drain distance, d_{vac}. Calculating the electric field in the vacuum barrier (diagonal gray lines in Figure 2a,b; for details see Supporting Information) reveals that $U_s(d_{vac})$ coincides with a constant field of 2.5 V/nm. The same applies for the gate voltage (U_G) of the transistor (Supporting Information, Figure S4), which we define as the potential difference between the single molecule and the source, and thus the voltage drop across the C_{60} bilayer $U_G = U_{C60}$. The field-dependent gating becomes even more obvious when the plasmonic light intensity and the source−drain current are plotted as a function of E and U_{bias} (insets Figure 2a,b), respectively. In order to account for the exponential decay of the tunnel current with increasing molecule−drain distance, the data in the insets of Figure 2a,b are divided by the current at the corresponding switching voltage U_S.

We can rationalize the strong response to the electric field by an analogy to a conventional field-effect transistor. In both devices, crossing of a specific gate voltage threshold opens a conduction channel between source and drain. In the following we show that in our case, however, the conduction channel is controlled via a particular electronic level of the quantum system, instead of the density of charge carriers. In this sense, the mechanism rather resembles a resonant tunneling transistor.[26] We exploit the fact that single $Ir(ppy)_3$ molecules adsorbed on a C_{60} bilayer possess an unoccupied state (violet bar, Figure 3a) close to the Fermi energy of the source electrode ($E^0_{Ir(ppy)3} \sim -0.5$ eV, for details see Supporting Information, Figure S5). Hence, the energy alignment of the single $Ir(ppy)_3$ molecules is markedly different to the situation on a C_{60} monolayer.[24] For finite bias voltages, this molecular state is shifted by the potential difference between the source contact and the single molecule, that is, the voltage drop (U_{C60}) across the C_{60} barrier (red bar, Figure 3).

At low electric field, the $Ir(ppy)_3$ state still lies above the Fermi level of the source electrode. In this case, electrons tunneling from the occupied C_{60} states lead to an only marginal tunnel current. However, these electrons cannot provide enough energy to excite plasmons. When the electric field is increased, for example, by decreasing d_{vac} at constant bias voltage, U_{C60} rises. As soon as $eU_{C60} = -E^0_{Ir(ppy)3}$ (Figure 3b), an electron from the source electrode tunnels through the source barrier and charges the single molecule. While the additional electron occupies the $Ir(ppy)_3$ state, its charge raises the potential of the single molecule by the corresponding Coulomb energy and thus inhibits the tunneling of a second electron from the source. Consequently, this process is quantum-limited. At the same time, the transistor turns on and opens two plasmon excitation channels: ① The additional electron can tunnel farther to the drain electrode and excite a plasmon in the junction. ② The additional charge on the single molecule leads to a local band bending[27] in the underlying C_{60} bilayer. This increases the energy of the electrons in the occupied C_{60} states, which now can also tunnel with energies high enough to excite plasmons. The contribution from channel ② becomes particularly apparent in constant height STM images. As visible in Figure 4, the single molecule is surrounded by an oval region of increased light intensity (Figure 4b) and current (Figure 4c) that is larger than the spatial extension of the involved $Ir(ppy)_3$

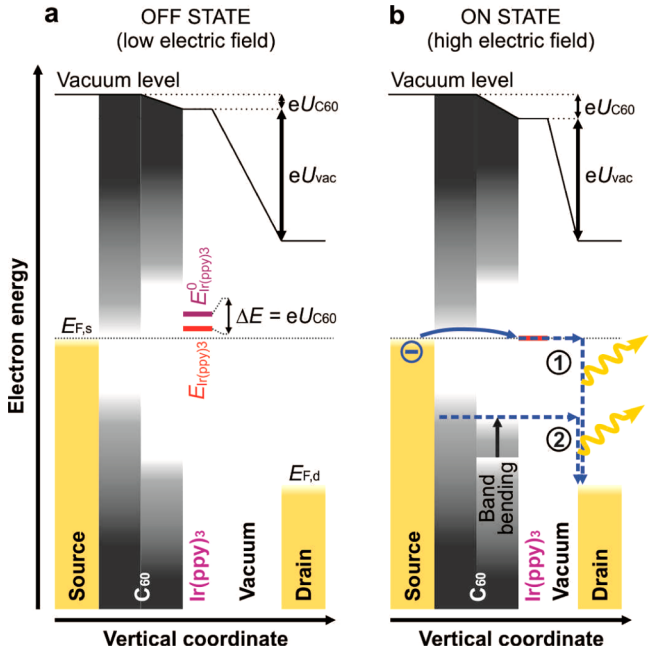

Figure 3. Gating mechanism and density of states of the junction. (a) OFF state and (b) ON state of the plasmon generation. The adsorbed $Ir(ppy)_3$ molecule possesses an unoccupied electronic state (violet bar) at an energy $E^0_{Ir(ppy)3}$ slightly above the Fermi level of the source contact, $E_{F,s}$. At positive source−drain voltages, the energy of this state is reduced ($E_{Ir(ppy)3}$, red bar) according to the voltage drop across the C_{60} layer, U_{C60}. (b) As soon as the $Ir(ppy)_3$ state reaches $E_{F,s}$, it becomes occupied by an electron from the source electrode and the transistor turns on. This opens two inelastic tunnel channels ① and ② that excite plasmons in the junction.

state (Figure 4a). Aside to the molecule, for example, at the white circle, tunneling through this state (channel ①) is not possible and all the current passes through the occupied C_{60} states. As long as the electric field at the single-molecule exceeds a threshold of 2.5 V/nm, however, the single-molecule remains charged and sustains the local band bending of the C_{60} bilayer (channel ②). In accordance with this interpretation, intensity−voltage curves and current−voltage curves recorded on adjacent C_{60} molecules next to the $Ir(ppy)_3$ state show a similar switching behavior as on top of the $Ir(ppy)_3$ state (Supporting Information, Figure S6). Furthermore, the areas of increased plasmonic light intensity and current both grow with increasing bias voltage and decreasing molecule−drain distance (Supporting Information, Figure S6). Consequently, the charging state of the quantum system can be monitored by the intensity of excited plasmons, either directly on top of the quantum system or indirectly at some distance away from it via the local band bending in the semiconducting C_{60} layer.

We note that when using silver instead of gold electrodes (Supporting Information, Figure S7), the charging of the $Ir(ppy)_3$ molecule occurs already at a bias voltage of about 1.5 V. At this voltage, the occupied C_{60} states lie below the Fermi energy of the drain and cannot contribute to the tunnel current, even when including their band bending. Thus, in this case plasmons are exclusively excited via the quantum-limited channel ①.

In order to determine the time response of the transistor, we repeatedly switched one single $Ir(ppy)_3$ molecule between its charged and neutral state by a continuous train of nanosecond voltage pulses.[28] In this experiment, the STM tip is positioned

dx.doi.org/10.1021/nl502413k | Nano Lett. 2014, 14, 5693−5697

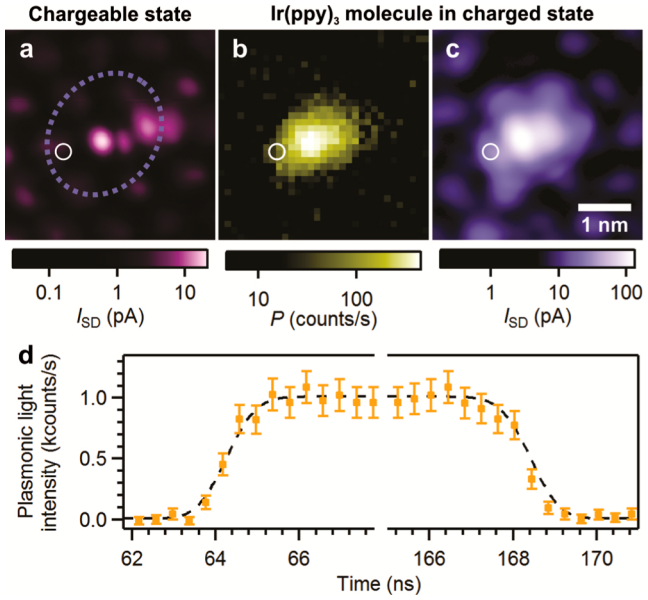

Figure 4. Spatial and temporal dependence of the plasmonic light emission. (a–c) Logarithmic plot of constant height STM maps of a single $Ir(ppy)_3$ molecule on a C_{60} bilayer on Au(111). (a) Spatial shape of the chargeable $Ir(ppy)_3$ state mapped by a current image (U_{bias} = 390 mV, d_{vac} = 0.4 nm). (b) Plasmonic light intensity, P and (c) simultaneously recorded current, I_{SD} (U_{bias} = 3.5 V, d_{vac} = 1.11 nm). The white circle in panels a–c indicate the same position on a C_{60} molecule next to the chargeable $Ir(ppy)_3$. The dotted oval in panel a marks the region of increased current in panel c due to the induced band bending of the C_{60} layer. (d) Time-resolved plasmonic response (yellow symbols, error bars show the statistical error) to a square voltage pulse (U_{bias}^{DC} = 2.85 V, U_{bias}^{AC} = 150 mV, $\langle I_{SD}\rangle$ = 10 pA) on top of a single $Ir(ppy)_3$ molecule. The dashed black line depicts the simulated trace of an instantaneous emission process considering the finite experimental time resolution (for details see Supporting Information, Figure S8). In panel b, the intensity is binned over 5 × 5 pixels.

at a constant height above the $Ir(ppy)_3$ molecule. The offset voltage is chosen to lie below the switching voltage (U_{bias}^{DC} = 2.85 V), while each voltage pulse (amplitude U_{bias}^{AC} = 150 mV) enables the charging of the single molecule. Figure 4d shows the time-resolved plasmonic light intensity (yellow symbols). For comparison, the dashed line in Figure 4d depicts the intensity expected for an instantaneous response, considering the finite experimental time resolution of 1.4 ns (for details see Supporting Information, Figure S8). The perfect agreement with the measured light intensity reveals that both the charging and discharging of the single molecule occur in less than 1 ns. Accordingly, the transistor could be driven well in the gigahertz-range. In fact, we expect that much higher clock rates might be realizable by using the concepts developed here, because both the charging of molecules[29] and the decay of surface plasmons[30] can occur on subpicosecond time scales.

In conclusion, we have demonstrated that an individual quantum system, consisting of a single molecule, is able to dynamically control the electrical plasmon generation in a tunnel junction. This enables both following subtle dynamic changes of the single quantum system itself via the detection of excited plasmons, as well as modulating the electrical plasmon generation at its quantum limit. For the example of a single $Ir(ppy)_3$ molecule, we have shown that the plasmon generation can be controlled over three decades with an electric field sensitivity of 11 mV/nm per decade (Figure 2a) and frequencies well in the gigahertz range. The described effect is expected to be applicable to a large variety of other quantum systems, such as quantum dots or even single atoms, as well as alternative barrier materials. In fact, the plasmon gating only relies on the relative alignment of a confined electronic state incorporated in a double tunnel barrier with respect to the contacting electrodes. The specific electronic structure of the junction thereby determines the number of plasmon excitation channels that are gated by the quantum system. Therefore, a skillful choice of the electronic structure of the junction allows the realization of electronically driven and ultrafast gateable single SPP sources. It will be the challenge of future studies to enhance and apply the demonstrated effects in planar tunnel junction and metal–insulator–metal waveguides. Such quantum interfaces, bridging nanoelectronics and nanophotonics, might provide new avenues to realize single-plasmon-on-demand sources and to convert electronic qbits into photonic qbits.

Methods. The experiments are performed with an in-house built, low temperature (4 K) ultrahigh vacuum (UHV, $<10^{-11}$ mbar) STM. The samples are prepared under UHV conditions by repeated sputtering and annealing of either a Au(111) or a Ag(111) crystal. For the subsequent thermal evaporation of a bilayer of C_{60} and a submonolayer coverage of $Ir(ppy)_3$, the substrate temperature is held at 320 and 240 K, respectively. *fac*-tris(2-phenylpyridine)iridium(III) is synthesized and purified as described elsewhere.[24] We have proven its non-destructive evaporation by laser desorption–ionization mass spectrometry on evaporated thin films. As STM tips, electrochemically etched gold tips are used. In the case of the measurements on a Ag(111) substrate, the tips were evaporated under UHV conditions with silver.

The photons emitted from the STM tunnel junction are guided by three lenses surrounding the STM tip to three independent detectors outside the vacuum chamber. For the experiments shown here, one of these optical ports is equipped with an optical spectrometer (Acton SP300i), another one with a spectrally integrating avalanche single photon counting diode (APD, PerkinElmer SPCM-AQRH-15). For all given values of the plasmonic light intensity, an experimentally determined APD dark count rate of 54 counts/s has been subtracted. Differential conductance (dI/dU) spectra and maps are recorded by using a lock-in technique and modulating the bias voltage (U_{mod} = 20 mV, f_{mod} = 500–800 Hz). All indicated voltages refer to the drain (STM tip) with respect to the grounded source (substrate).

For the time-resolved measurements, a continuous train of square voltage pulses (t_p = 100 ns, U_{bias}^{AC} = 150 mV, duty cycle 33%) from an arbitrary waveform generator (Agilent M8190A) is added by a bias-tee to a constant voltage of U_{bias}^{DC} = 2.85 V and sent to the tunnel junction. Details can be found in ref 28.

The drift of the source–drain distance (vertical STM tip position) during the acquisition of the data shown in Figure 2 is corrected by repeatedly measuring the current on the same C_{60} molecule several nanometers away from the single $Ir(ppy)_3$ molecule at the same nominal source–drain distance and bias voltage (5 data points during 2.5 h). The measured time-dependent current is then fitted by an exponential function. By assuming a 1 order of magnitude change in current for a 0.1 nm displacement, the drift can be estimated from the fitted exponent. The resulting vertical drift during the data acquisition of Figure 2 is (−81 ± 5) pm/h. The lateral drift has been corrected during the measurement, by adjusting the lateral

dx.doi.org/10.1021/nl502413k | *Nano Lett.* 2014, 14, 5693–5697

STM tip position in between the acquired tunneling spectra to the highest point on the single $Ir(ppy)_3$ molecule.

■ ASSOCIATED CONTENT

Supporting Information

Calculation of the voltage drop across the C_{60} barrier and the electric field, spectrum of radiated light, determination of absolute molecule−drain distances, current and plasmonic light intensity as a function of gate voltage, dI/dU spectra of $Ir(ppy)_3$ adsorbed on a C_{60} bilayer on Au(111) and Ag(111), mapping of the C_{60} band bending, and measured and simulated plasmonic time response. This material is available free of charge via the Internet at http://pubs.acs.org.

■ AUTHOR INFORMATION

Corresponding Author

*E-mail: c.grosse@fkf.mpg.de.

Author Contributions

K.Ke., K.Ku., and U.S. conceived and directed the project. C.G., A.K., T.L., R.F., M.E., and K.Ku. performed the experiments and analyzed the data. F.S. and M.R. synthesized and purified $Ir(ppy)_3$. C.G. wrote the manuscript with input from all authors.

Notes

The authors declare no competing financial interest.

■ ACKNOWLEDGMENTS

We thank K. Amsharov and S. Rauschenbach for the characterization of evaporated $Ir(ppy)_3$ films by laser desorption−ionization mass spectrometry and S. Loth for discussions and valuable help on the time-resolved measurements. U.S. acknowledges funding by the Emmy-Noether-Program of the Deutsche Forschungsgemeinschaft.

■ ABBREVIATIONS

dI/dU spectra/maps, differential conductance spectra/maps; $Ir(ppy)_3$, *fac*-tris(2-phenylpyridine)iridium(III); STM, scanning tunneling microscopy; SPP, surface plasmon polariton

■ REFERENCES

(1) Takahara, J.; Yamagishi, S.; Taki, H.; Morimoto, A.; Kobayashi, T. *Opt. Lett.* **1997**, *22* (7), 475−477.
(2) Gramotnev, D. K.; Bozhevolnyi, S. *Nat. Photonics* **2010**, *4* (2), 83−91.
(3) Schuller, J. A.; Barnard, E. S.; Cai, W.; Jun, Y. C.; White, J. S.; Brongersam, M. L. *Nat. Mater.* **2010**, *9* (3), 193−204.
(4) Ozbay, E. *Science* **2006**, *311* (5758), 189−193.
(5) Sorger, V. J.; Oulton, R. F.; Ma, R.-M.; Zhang, X. *MRS Bull.* **2012**, *37* (8), 728−738.
(6) Anker, J. N.; Hall, W. P.; Lyandres, O.; Shah, N. C.; Zhao, J.; Van Duyne, R. P. *Nat. Mater.* **2008**, *7* (6), 442−453.
(7) Kolesov, R.; Grotz, B.; Balasubramanian, G.; Stoehr, R. J.; Nicolet, A. A. L.; Hemmer, P. R.; Jelezko, F.; Wrachtrup, J. *Nat. Phys.* **2009**, *5* (7), 470−474.
(8) Akimov, A. V.; Mukherjee, A.; Yu, C. L.; Chang, D. E.; Zibrov, A. S.; Hemmer, P. R.; Park, H.; Lukin, M. D. *Nature* **2007**, *450* (7168), 402−406.
(9) Jacob, Z.; Shalaev, V. M. *Science* **2011**, *334* (6055), 463−464.
(10) Tame, M. S.; McEnery, K. R.; Ozdemir, S. K.; Lee, J.; Maier, S. A.; Kim, M. S. *Nat. Phys.* **2013**, *9* (6), 329−340.
(11) de Leon, N. P.; Lukin, M. D.; Park, H. *IEEE J. Sel. Top. Quantum Electron.* **2012**, *18* (6), 1781−1791.
(12) Weber, W. H.; Eagen, C. F. *Opt. Lett.* **1979**, *4* (8), 236−238.
(13) Koller, D. M.; Hohenau, A. D. H.; Galler, N.; Reil, F.; Aussenegg, F. R.; Leitner, A.; List, E. J. W.; Krenn, J. R. *Nature Phot.* **2008**, *2* (11), 4.
(14) Neutens, P.; Lagae, L.; Borghs, G.; Van Dorpe, P. *Nano Lett.* **2010**, *10* (4), 1429−1432.
(15) Walters, R. J.; van Loon, R. V. A.; Brunets, I.; Schmitz, J.; Polman, A. *Nat. Mater.* **2010**, *9* (1), 21−25.
(16) Huang, K. C. Y.; Seo, M.-K.; Sarmiento, T.; Huo, Y.; Harris, J. S.; Brongersma, M. L. *Nat. Photonics* **2014**, *8* (3), 244−249.
(17) Rai, P.; Hartmann, N.; Berthelot, J.; Arocas, J.; des Francs, G. C.; Hartschuh, A.; Bouhelier, A. *Phys. Rev. Lett.* **2013**, *111*, 020401.
(18) Lambe, J.; McCarthy, S. L. *Phys. Rev. Lett.* **1976**, *37* (14), 923.
(19) Gimzewski, J. K.; Sass, J. K.; Schlitter, R. R.; Schott, J. *Europhys. Lett.* **1989**, *8* (5), 435−440.
(20) Berndt, R.; Gaisch, R.; Schneider, W.-D.; Gimzewski, J. K.; Reihl, B.; Schlittler, R. R.; Tschudy, M. *Phys. Rev. Lett.* **1995**, *74* (1), 102−105.
(21) Wang, T.; Boer-Duchemin, E.; Zhang, Y.; Comtet, G.; Dujardin, G. *Nanotechnology* **2011**, *22*, 175201.
(22) Bharadwaj, P.; Bouhelier, A.; Novotny, L. *Phys. Rev. Lett.* **2011**, *106* (22), 226802.
(23) Beams, R.; Bharadwaj, P.; Novotny, L. *Nanotechnology* **2014**, *25*, 055206.
(24) Lutz, T.; Große, C.; Dette, C.; Kabakchiev, A.; Schramm, F.; Ruben, M.; Gutzler, R.; Kuhnke, K.; Schlickum, U.; Kern, K. *Nano Lett.* **2013**, *13*, 2846.
(25) Piva, P. G.; DiLabio, G. A.; Pitters, J. L.; Zikovsky, J.; Rezeq, M.; Dogel, S.; Hofer, W. A.; Wolkow, R. A. *Nature* **2005**, *435* (7042), 658−661.
(26) Capasso, F.; Kiehl, R. A. *J. Appl. Phys.* **1985**, *58* (3), 1366−1368.
(27) Pradhan, N. A.; Liu, N.; Silien, C.; Ho, W. *Phys. Rev. Lett.* **2005**, *94* (7), 076801.
(28) Grosse, C.; Etzkorn, M.; Kuhnke, K.; Loth, S.; Kern, K. *Appl. Phys. Lett.* **2013**, *103*, 183108.
(29) Hannappel, T.; Burfeindt, B.; Storck, W.; Willig, F. *J. Phys. Chem. B* **1997**, *101* (35), 6799−6802.
(30) Keil, U. D.; Ha, T.; Jensen, J. R.; Hvam, J. M. *Appl. Phys. Lett.* **1998**, *72* (23), 3074−3076.